“SUPPORTING INFORMATION”

Unscrambling the influence of sodium cation on the structure, bioactivity and erythrocyte compatibility of 45S5® bioactive glass

Vijayakumari Sugumaran[1], Elakkiya Krishnamoorthy[1], Annamalai Kamalakkannan[1], Riju Chandran Ramachandran[1], Balakumar Subramanian[1*]

[1]*National Centre for Nanoscience and Nanotechnology, University of Madras, Guindy Campus, Chennai – 600025, Tamilnadu.*

* Corresponding author E-mail: balasuga@yahoo.com

1. Materials and Methods

1.1 *In-vitro* Mineralization studies

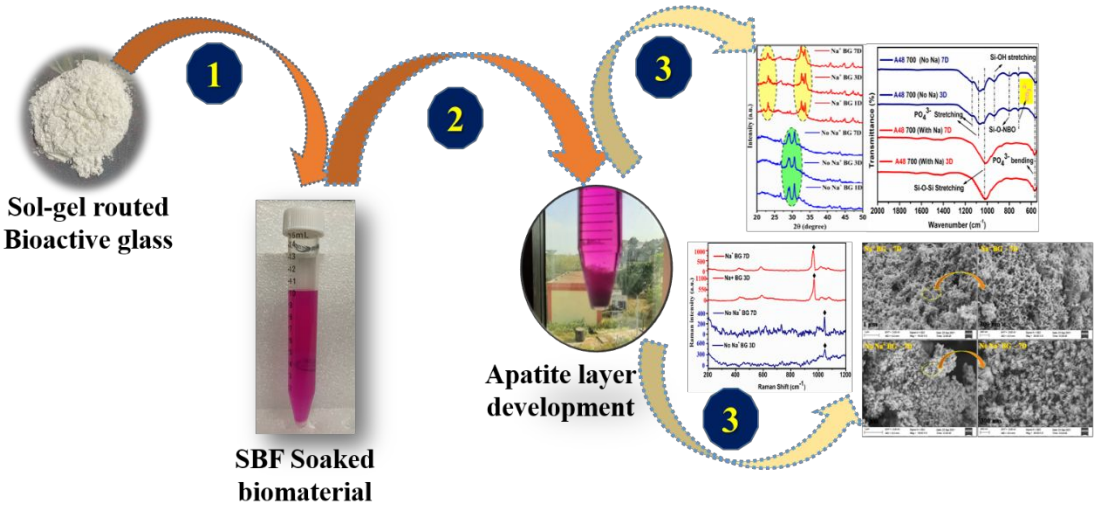

Figure S1. Pictorial demonstration of *in-vitro* studies carried out in simulated body fluid (SBF) by soaking 100mg of the prepared the bioactive glass.

Table T1. Comparative figures on concentration of Ions in SBF & Human plasma [1]

Ions Concentration (mM) in SBF & Human Plasma								
Ions	**Na^+**	**K^+**	**Mg^{2+}**	**Ca^{2+}**	**Cl^-**	**HCO_3^-**	**HPO_4^{2-}**	**SO_4^{2-}**
SBF	142.0	5.0	1.5	2.5	147.8	4.2	1.0	0.5
Human Plasma	142.0	5.0	1.5	2.5	103.0	27.0	1.0	0.5

2. Result and Discussion

2.1 Thermal Analysis:

Table T2. Thermal Profile of the prepared BG

Thermogravimetric Analysis (TG)				
Sample	**Stages**	**Temperature range (°C)**	**Mass loss (%)**	**Overall mass loss (%)**
Na^+ BG	**I**	**31.8 - 325.17**	**11.24%**	**53.26%**
	II	**355.17 - 598.90**	**7.26%**	

	III	**589.90 – 797.25**	**34.76%**	
No Na^+ BG	**A**	**31.8 – 157.5**	**18.56%**	**35.59%**
	B	**157.5 – 333.5**	**6.04%**	
	C	**333.5 – 596.19**	**10.99%**	

Differential Thermal Analysis (DTA) & Derivative Thermo-gravimetric Analysis (DTG)

Sample	**Stages**	**Major loss at temperature (°C)**		**Decomposed Solid**	**Reference**
Na^+ BG	a	124°C	**Δ**	Removal of physisorbed water & evaporation of organic compounds including ethanol	[2]
	b	296.09°C	**ΔΔ**	Elimination of Alkoxy groups and chemisorbed water molecules	[5]
	c	Between 711.15°C and 749.8°C	□ □□	Phase crystallization of dominant phase $Na_2CaSi_2O_6$ & β-$Na_2Ca_4(PO_4)_2SiO_4$	[3,4]
No Na^+ BG	i	Between 102°C and 138°C	**Δ**	Removal of physisorbed water & evaporation of organic compounds including ethanol	[2]
	ii	Between 359.7°C and 420°C	**ΔΔ**	Elimination of Alkoxy groups and chemisorbed water molecules	[5]
	iii	Between 550°C and 570°C	♦	Glass transition temperature, crystallization of amorphous $CaCO_3$ phase and onset of a dominant phase crystallization.	[6,33]

2.2 Surface functional group analysis via FTIR:

The functional modes of the synthesized bioactive glass also for the same after immersion in Simulated Body Fluid for 3 days and 7 days have been recorded and shown in figure 4. In addition to the influence of sodium monovalent cation, increasing ageing time for 48 hours also influences the stretching and bending between the molecules.

Interestingly, Fourier Transform Infrared spectroscopy **(**FTIR) spectral analysis evidences that, 48 hours ageing process of the sol with the absence of monovalent cation (No

Na^+ BG), naturally results in the formation of apatite like phase as observed in XRD even before immersed in simulated body fluid. The above phrase is corroborated by the set of transmittance bands detected at 1789cm^{-1}, 1637 cm^{-1}, 1529 cm^{-1} which corresponds to presence of carbonates, C-O bending or H-O-H bending due to water absorption and C-O stretching from CO_3^{2-} ions respectively [7,8,9,10]. The CO_3^{2-} antisymmetric bending is also found from 1444 cm^{-1} band [11] and these peaks are also observed in directly synthesized hydroxyapatite biomaterials. As stated by Aguilar-Reyes et. al, [22] the atmospheric CO_2 and /or dissolved CO_2 is being absorbed by the sample during ageing and resulted in the emergence of carbonate peaks. On the contrary, the above mentioned bands are not observed in sodium containing bioactive glass i.e., in Na^+ BG. Therefore, it is predicted that atmospheric CO_2 dissolution in the sol while engineering the bioactive glass is being guarded by the monovalent cations. The band at 1345 cm^{-1} is reported as the bond between carboxyl group and the Ca^{2+} ions from the Hydroxyapatite [23]. This result shows good agreement with XRD data where apatite phase is observed for the sample devoid of sodium cations. Looking into the hydrolysis, condensation and polymerization mechanisms of TEOS as proposed by Karmar, 2016 [12], Silicic acid is a product on complete hydrolysis of TEOS after the elimination of ethanol molecules.

$$Si(OC_2H_5)_4 + 4H_2O \rightarrow Si(OH)_4 + 4C_2H_5OH \quad (1)$$

Then, siloxane ≡Si-O-Si≡ is formed on the condensation reaction between the molecules of silanol groups by excluding a water molecule and the reaction can be given as

$$2(OC_2H_5)_3SiOH \rightarrow (OC_2H_5)_3Si - O - Si(OC_2H_5)_3 + H_2O \quad (2)$$

Simultaneously, on the other hand, silanols and ethoxy groups condensed to form siloxane ≡Si-O-Si≡ by excluding a molecule of ethanol.

$$(OC_2H_5)_3SiOH + C_2H_5O\text{-}Si(OC_2H_5)_3 \rightarrow (OC_2H_5)_3Si - O - Si(OC_2H_5)_3 + C_2H_5OH \quad (3)$$

From the above equations, it can be assumed that O-H and/or OH^- groups found a magnificent place in No Na^+ BG or may be due to C-H bend [13] and resulted in higher intense band at 1345 cm^{-1} projecting not only carboxyl group, even hydroxyl group can result this band.

The asymmetric vibrational mode at 1224 cm^{-1} labels the metaphosphate group (PO_2) deprived of bridging oxygens [14]. The P= O stretching's are observed at 1142 cm^{-1} in Na^+ BG and at 1151 cm^{-1} for No Na^+ BG [15]. The difference in band shifts are assumed to be based on the fact that lower molecular mass results in peaks shift to higher wavenumber. Thus, vibrational frequency is directly proportional to lighter the molecule, therefore higher the wavenumber [12].

For SiO_2 comprising bio-glasses, the bands at 1078 cm^{-1}, 1083 cm^{-1} are attributed to asymmetric stretching vibration of Si-O-Si linkage or Si – O^- units [12, 15, 16]. The samples after being immersed in the simulated body fluid up to 7 days exposes similar P=O and Si-O-Si with shift to lower wavenumbers that are observed at 1139 cm^{-1} and 1180 cm^{-1} representing P=O and Si – O^- respectively [15]. The shift is because phosphates are released from the silica matrix and resulted in increase in mass of precipitation towards formation of hydroxycarbonate apatite (HCA) layer; simultaneously silanols are formed on reaction of Si-O- groups with H^+ ions in the SBF for the sodium free samples. The band at 1033 cm^{-1} is assigned for P- O stretching and may also for bridging oxygen of Si-O-Si asymmetric stretching surrounding the silica tetrahedra and/or Si-O^- non-bridging oxygen bands [6,16,20]. X.Chatzistavrou et. al., [6] pointed that owing to the overlapping of PO_4 stretching in the range 1100-1050 cm^{-1}, Si-O-Si asymmetric stretching is very strong, and those results are correlated to the spectra for monovalent cation containing bioglass (Na^+ BG). One of the important characteristic bands representing the crystalline phosphate layer is observed at 1025.7 cm^{-1} for both the immersed samples with and without sodium cation [21] as shown in fig. 5(b). This clears that even without sodium monovalent cation, crystalline phosphate hydroxycarbonate apatite can be achieved. The IR bands at 940 cm^{-1}, 954 cm^{-1} before immersion and at 933 cm^{-1} after immersion corresponds to Si-O-2NBO stretching highly indicating the ability of sample to form silanol group (Si-OH) which assist as a nucleation site for HCA precipitation. Also, the aforementioned band 933 cm^{-1} symbolizes $Na_2CaSi_2O_6$ phase in accordance with XRD results [4]. These silanols persuades the precipitation of HCA layer [19,15]. Caciotti et. al [17] predicts that 933 cm^{-1} may also be due to Si-O-Ca bending where Si-O-Na is impossible owing to the non-availability of sodium ion in our case. Here, the monovalent cation free bioactive glass (No Na^+ BG) exhibits such a band on immersion for 3 days and 7 days in SBF but not in Na^+ BG sample. Regina et.al. [15] pointed out that region between 800 and 890 cm^{-1} features the C-O stretching which is observed on both the samples before immersion but not in No Na^+ BG after immersion. As per the statement of Caciotti et. al, [17] increasing in silanol groups and fading carbonate bands need to be correlated and the study conveyed that carbonation phenomena is not promising when more number of NBOs are bonded with cations. Henceforth, carbonates in the sodium free samples are utilized for the hydroxycarbonate apatite layer formation indirectly illustrating more NBO are bonded with calcium cations. Also it is evident that, not only carbonates formation, even NBOs elucidates the ability to form HCA layer. It is predicted that these Si-NBO-Ca bending might be a reason for the sodium free sample to exhibit higher hemostatic activity.

IR band centered at 720 cm^{-1} for Na^+ and 787 cm^{-1} for No Na^+ BG expose the symmetric stretching of Si-O-Si molecules whose tetrahedrons are surrounded by oxygen molecules. On immersion in SBF, No Na^+ BG alone retained such band with shift in wavenumbers indicating the earlier precipitation of HA usually occur at stage 3 as described by H.A. El Batal et.al [16] whose results are highly correlated with SEM micrographs. CO_2 absorbed onto the surface by sodium containing Bioglass is proven by the band at 664 cm^{-1} exhibiting as C-O asymmetric stretching vibrations [18]. The IR bending in the range 500-610 cm^{-1} represents the P-O that decides hydroxyapatite precipitation ability and considering as the signature bands [16]. Favorably, these bending are observed in this study provided with both amorphous and crystallized single bond P-O bending. Here, 579 cm^{-1}, 530 cm^{-1} in Na^+ BG specifically publicized the formation of silicorhenanite phase highly correlated with XRD results [4]. As silicorhenanite phase is isostructural to apatite phase, crystallized P-O bending representing HA is noticeable after immersion in SBF. Chen et.al, [20] clarifies that the apatite like phase formation and degradation of bioglass is conveyed through reduction in phosphate peaks after immersion. This is owing to the balanced reaction of ionic charge in orthophosphates by Na^+ ions and at times Ca^{2+} balances the charge in majority of orthophosphates for apatite crystallization. Thus, in this study, phosphate peaks are reduced and contribution of Ca^{2+} cation in No Na^+ BG to balance the charge in orthophosphates are evident. In view of that, sodium free sample favors higher precipitation of hydroxycarbonate apatite whose carbonate presence is highly correlated to XRD results. The wavenumbers and their assigned vibrational modes are tabulated in Table T3.

Table T3. IR Vibrational modes of Na^+ BG and No Na^+ BG

Wave number (cm^{-1})		**IR Vibrational Mode**	**Reference**
Na^+ BG	**No Na^+ BG**		
BEFORE IMMERSION			
-	1789 cm^{-1}	CO_3^{2-} group	[7]
-	1637 cm^{-1}	C-O bending from CO_3^{2-} ions and/or H-O-H bending	[8,9,18]
-	1529 cm^{-1}	C-O stretching vibration	[10]
-	1444.7 cm^{-1}	CO_3^{2-} antisymmetric	[11]
-	1345.04 cm^{-1}	O-H group and/or C-H bending	[13]
-	1224.66 cm^{-1}	Q_2 (PO_2) asymmetric	[14]
1142 cm^{-1}	1151.35 cm^{-1}	P= O stretching's	[15]
1078 cm^{-1}	1083.85 cm^{-1}	Si – O^- units asymmetric stretching	[12,15,16]
1033 cm^{-1}	-	Si-O-Si asymmetric stretching	[19,6,16]

940.2 cm^{-1}	954.87 cm^{-1}	Si-O-2NBO stretching and/or Si-NBO-Ca bending	[15,17]
814 cm^{-1}	887.37 cm^{-1}	C-O Stretching	[15]
	834 cm^{-1}		
720 cm^{-1}	787 cm^{-1}	Si-O-Si symmetric stretching whose tetrahedral is bounded by bridging oxygens	[16]
664.5 cm^{-1}	-	C-O Asymmetric stretching	[18]
579.5 cm^{-1}	567.7 cm^{-1}	P-O bending (amorphous)	[16]
555.89 cm^{-1}	550 cm^{-1}	P-O bending (crystal); revealing Silicorhenanite phase	[4,16]
530 cm^{-1}	536.7 cm^{-1}		
517 cm^{-1}	520, 512 cm^{-1}		
506 cm^{-1}	509 cm^{-1}		
AFTER IMMERSION			
-	1139 cm^{-1}	P= O stretching's	[15]
-	1080 cm^{-1}	Si-OH stretching's	[15]
1025.7 cm^{-1}	1025.7 cm^{-1}	Crystalline phosphate surface	[21]
-	933.73 cm^{-1}	Si-O-2NBO stretching and/or Si-NBO-Ca bending; revealing $Na_2CaSi_2O_6$ phase	[4, 19,15,17]
871.34 cm^{-1}	-	C-O Stretching	[15]
-	797.81 cm^{-1}	Si-O-Si symmetric stretching whose tetrahedral is bounded by bridging oxygens	[15,16]
-	713.16 cm^{-1}		
606.53 cm^{-1}	-	asymmetric P-O bending (HA)	[19]
569.9 cm^{-1}	566.1 cm^{-1}	Crystalline asymmetric P-O bending (HA)	[16,19]

2.3 Vibrational mode analysis via Raman Spectroscopy:

Table T4. Classification of Q^n species of silica and phosphate tetrahedrons possible in bioactive glass.

Species	Attribution	Anionic structural unit
$Q^0(P)$	Phosphate species	Orthophosphate form PO_4^{3-}
$Q^1(P)$	Phosphate species	$P_2O_7^{4-}$
$Q^2(P)$	Phosphate species	Metaphosphate PO^{3-} chain
$Q^3(P)$	Phosphate species	P_2O_5 i.e., P = O
$Q^4(P)$	Phosphate species	Stable phosphate form
RBO-Q^n	n = 1 to 3	Rocking motion of Bridging oxygen in Q^n that contain non-bridging oxygen.
Q^n (Si+P)	Si-O-P linkage	SiO_4 and PO_4 cross-connective Q species

Q^o	Single SiO_4 unit bonded with no other silica terahedrons	Orthosilicate unit SiO_4^{4-}
Q^1	Single SiO_4 unit bonded with one silica terahedron	Disilicate unit $Si_2O_7^{6-}$
Q^2	Single SiO_4 unit bonded with two silica terahedron	Metasilicate unit $Si_2O_6^{4-}$
Q^3	Single SiO_4 unit bonded with three silica terahedron	Phyllosilicate unit $Si_2O_5^{2-}$
Q^4	Single SiO_4 unit bonded by silica tetrahedron on all sides.	Stable silicate form

Table T5. Raman Vibrations of the prepared BG and their Attributions

Wave number (cm^{-1})		**RAMAN vibrational mode**	**Reference**
Na^+ BG	**No Na^+ BG**		
-	400	O-P-O Bending modes of PO_2 group	[27]
427.98	432.86	w_1 band	[25]
451	-	Si-O-Si rocking	[25]
-	485	D1	[25]
592±4	592±4	ν_4 PO_4^{3-} Stretching	[25]
-	732.3 ±1	Q^3 phyllosilicate unit $Si_2O_5^{2-}$	[24]
940	-	Q^o (P) symmetric stretching / PO_4^{3-} Stretching	[24,25]
966.8	966.8	PO_4^{3-} Stretching / Q2 Si-O-NBO	[24,25,26]
1027	-	Asymmetric stretching vibration of BOs in all Q species	[24]
1049	1047	ν_3 PO_4^{3-} asymm. Stretching + Si – O vibration	[24,25]
1082	1082	ν_3 PO_4^{3-} overlapped with ν_1 CO_3^{2-} / Q^3 symmetric stretching	[24]
-	1118.4	Si-O-Si stretching	[25]
-	1165.6	Q4 Si-O-Si asymmetric stretching, Si-O-Si = 160°	[24]

2.4 X-ray Photoelectron Spectroscopic Analysis (XPS):

Table. T6 Atomic Concentration Profile of the prepared Na^+ BG and No Na^+ BG

Atomic Concentration (%)					
	Si	**P**	**Ca**	**Na**	**O**

No Na^+ BG	**20.32**	**2.38**	**6.03**	**-**	**69.77**
Na^+ BG	**10.74**	**0.56**	**3.76**	**15.17**	**71.27**

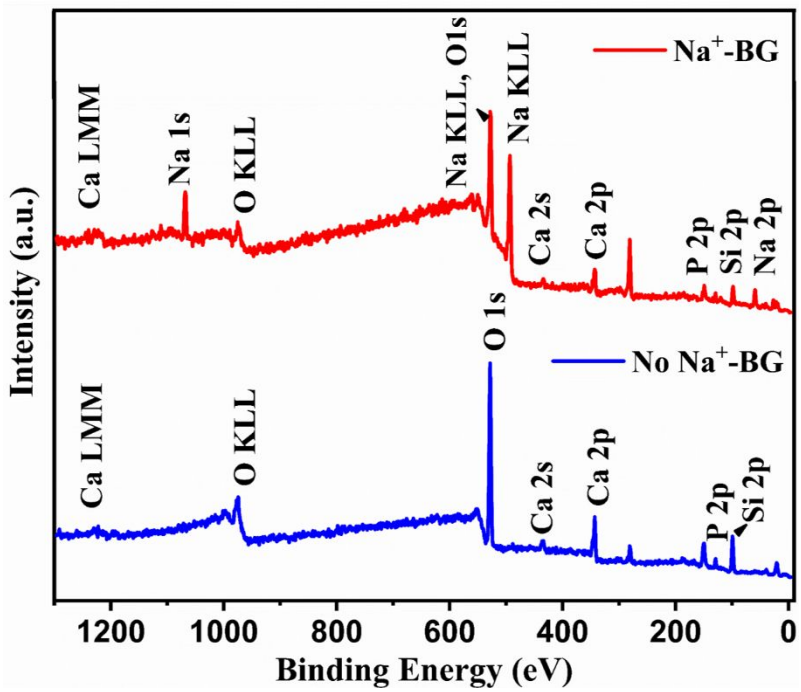

Figure. S2 XPS survey spectrum of Na^+ BG and No Na^+ BG confirming absence of sodium ion in No Na^+ BG

2.5 Surface Morphological Analysis via SEM, Fe-SEM:

By looking into the mechanism of hydroxyapatite-like layer formation over the surface of bio-active glass, Na^+ ions and Ca^{2+} ions from the surface are readily exchanged by H^+ ions in the fluid, resulting in surface silanols formation and further poly-condense to form silica gel layer. Marco Araujo et al., [28] reported that these layer combines with calcium ions and reacts with phosphate ions from the SBF and form amorphous calcium phosphate of lower Ca/P ratio. This amorphous layer further crystallizes and turns to phase of bone-like apatite with increase in Ca/P ratio. It is evident from EDAX, Ca/P ratio for Na^+ BG is 2.07 and No Na^+ BG is 1.29. Based on the mechanism, increase in bioactivity rely on the ratio of Ca/P ratio also [28]. If poorer the Ca/P ratio, greater will be bioactivity resulting in $Ca_3(PO_4)_2$ complexes formation on the silica gel layer and eventually, the migration of Ca^{2+} and PO_4^{3-} ions from solution gets facilitated. Thus, the crystallization of hydroxycarbonate apatite layer enhanced abruptly, favoring the increase in bioactivity of the glass network. Hence, whenever the atomic ratio of Ca/P < 1.67, the formed layer is calcium deficient type apatite, and Ca/P >1.67 is calcium rich apatite but not stoichiometric hydroxyapatite [28, 29]. Therefore, it is concluded that Na^+ BG provides calcium rich apatite; whereas calcium deficient apatite is formed by Na^+ free BG because Ca^{2+} ions prefer

to bond with non-bridging oxygens (NBOs) of phosphate ions than silicates. Therefore, migration of maximum Ca^{2+} ions are restricted by phosphate species, as it holds more of Ca^{2+} to bond with NBOs, resulting in the formation of calcium deficient apatite layer as observed in No Na^{+} BG.

Meanwhile, Catauro et.al, [57] pointed that calcium deficient apatite layer is similar to bone- apatite as it has low Ca/P ratio. Thus, it is assumed that No Na^{+} BG binds with bone strongly than Na^{+} BG even though it exhibits calcium rich apatite because higher the Ca/P ratio than 1.67, lower will be the bone-material bonding.

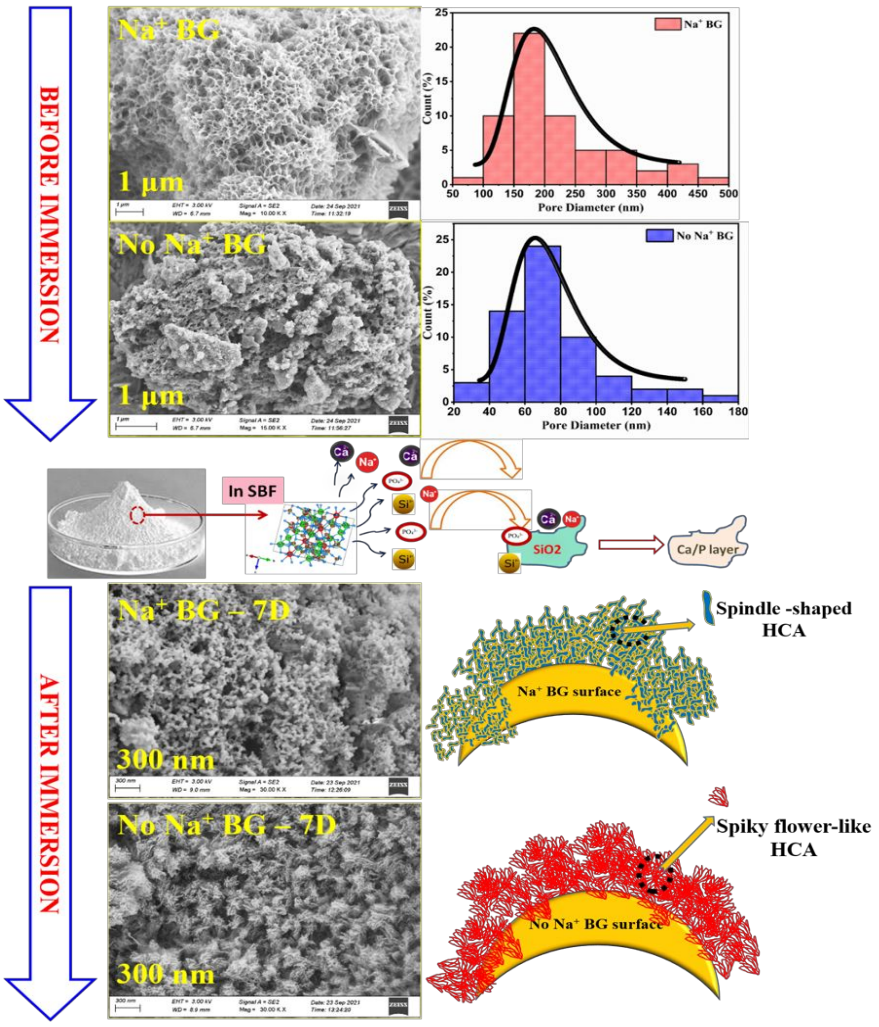

Figure S3. FE-SEM Micrographs of Na^{+} BG and No Na^{+} BG before and after immersion showing enhanced apatite growth; Average particle size distribution curves projecting 180 nm for Na^{+} BG and 65nm for No Na+ BG; Schematic representation of developed apatite morphology over the surface of bioactive glasses.

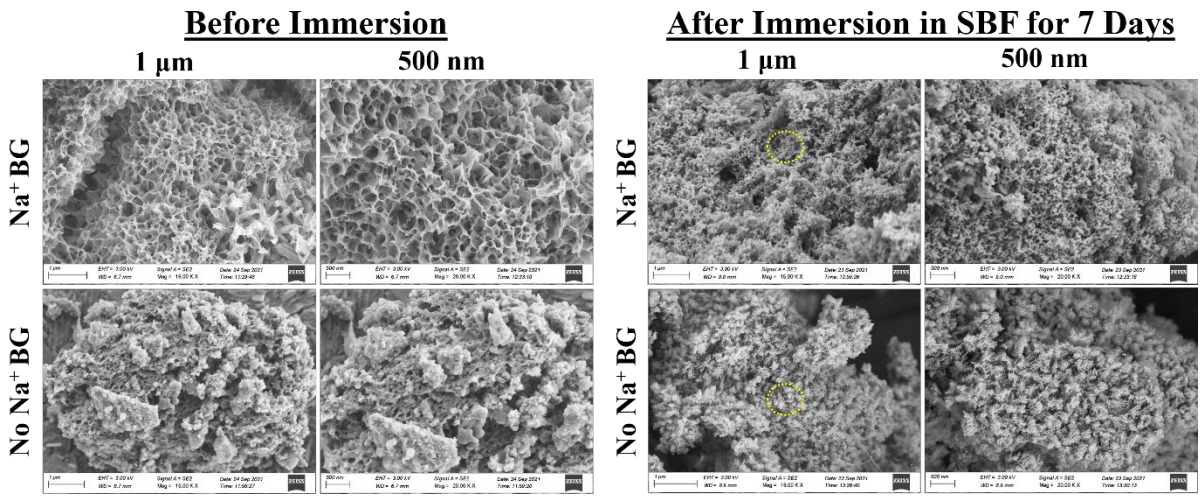

Figure S3-A. Magnified FE-SEM Micrographs of Na^+ BG and No Na^+ BG before and after immersion. After immersion in SBF for 7 days, Na^+ BG shows spindle shaped hydroxyl carbonate apatite (HCA) growth whereas No Na+ BG shows spiky flower like HCA growth.

2.6 pH studies:

Generally, it is well-known that the influence of network modifying cation could increase the pH of the medium when in contact with the fluid. Armed with the knowledge of mechanism, modifying cations from the bioactive material undergo rapid exchange with H^+ ions of the fluid by increasing pH of the medium. Thus, when the bioactive materials of 100mg is soaked in simulated body fluid (SBF) for subsequent days, pH of the solution drastically increases for Day 1 and gradually decreases for Day 3 and Day 7 as seen in fig.8(a). Herein, control denotes the pure simulated body fluid without the material with pH 7.4. Simultaneously, pH increases to 8.64 for the sample devoid of sodium cation and super-saturated at Day 3 and Day 7 whose pH is almost constant denoting the decrement in exchange of ions between the surface of the sample and fluid.

Marco Araujo et. al. [28] stated that lower pH value is possible not only because of increase in P_2O_5 content but also due to decrease in number of modifier cation in the glass network. Also, Ca^{2+} ions who coordinated more with NBOs of phosphate species than silicates, might indorsed this lower pH maintenance [30]. Hence, it is evident from the study that, even Ca^{2+} can increase the pH and an equal release of phosphate ions from No Na^+ BG buffers this alkalinity change ensuing lower pH level. According to R.G.Hill et. al.,[31] apatite formation can be achievable by the release of Ca^{2+} ions by means of super saturation of the medium powered with calcium and phosphate ions and also Na^+ ions does not influence the bioactivity. On the other hand, Na^+ ions exchanges more rapidly with H^+ ions from the SBF solution

promoting pH increase in the medium favored by glass network weakening. It can be concluded that, sodium monovalent cation free bioactive glass can also exhibit appreciable bioactivity and superior biocompatibility.

2.7 Network Connectivity:

Considering SiO_2 and P_2O_5 are network forming groups, the average bridging oxygens bonded per network former ion decides the Network connectivity (NC). Higher the Network connectivity, lower would be the degradation of the biomaterial [31]. Assuming phosphorous occurs in orthophosphate form [PO_4^{3-}], network connectivity can be calculated theoretically by using the relation,

$$NC = \frac{4[SiO_2] - 2[Na_2O + CaO] + 6\,[P_2O_5]}{[SiO_2\,]}$$

where, mono- and divalent modifier are Na_2O and CaO in the glass network

As shown in fig.15. NC was calculated using equation (1) as NC=2.11 for Na^+ BG and NC = 3.17 for No Na^+ BG by means of Mole percent substitutions, where mole percent substitutions gains higher significance over structure level [32]. Higher glass solubility is seen in lower Network connectivity sample; thus, in our case, Na^+ BG degrades more easily than No Na^+ BG and the results are highly correlated with Vicker's hardness. It is because Na_2O cation content weakens the glass network by creating expansion, results in decrement in both oxygen density and glass density proving to be a highly reactive network disruptive species [32]. Thus, sodium monovalent cation free sample results as higher stable bioactive material that can be used in ortho- and dental application.

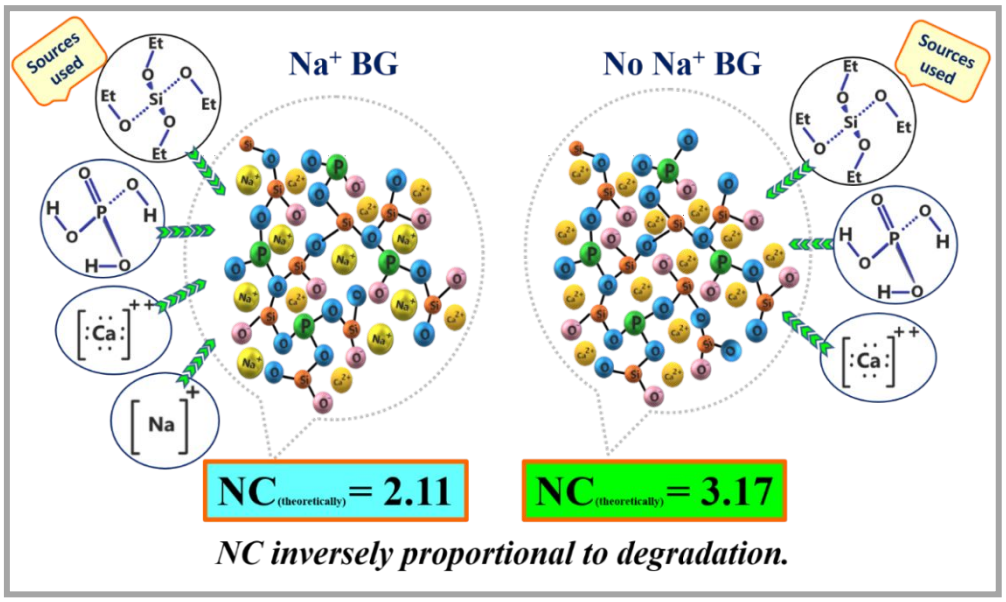

Figure S4. Pictorial projection of Network connectivity of Na^+ BG and No Na^+ BG

2.8 Mechanical and Stability test:

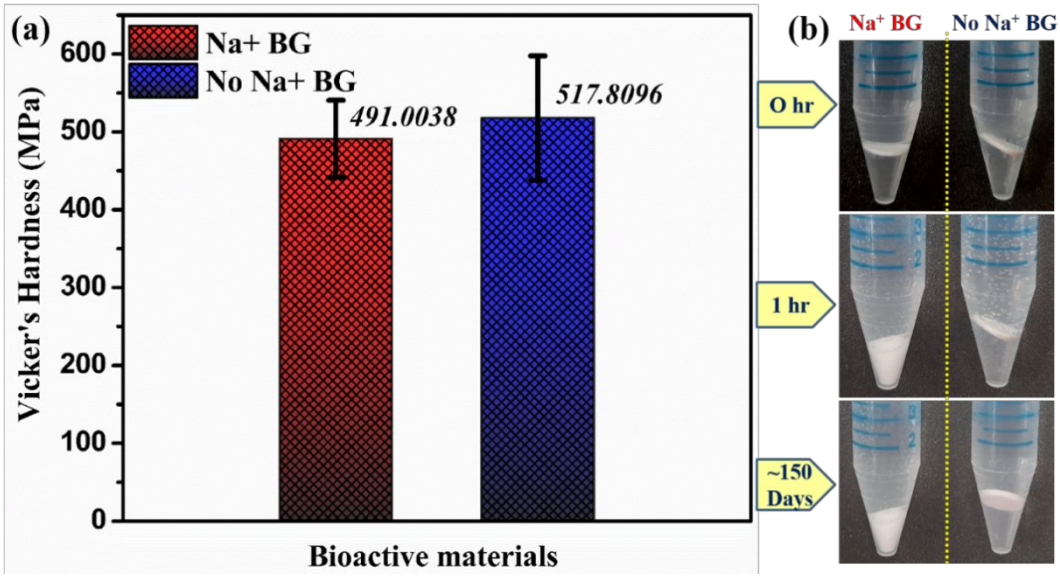

Figure S5. a) Micro-hardness results of Na^+ BG and No Na^+ BG; b) Experimental proof on stability of No Na^+ BG that can withstand for more than 150 days on soaking in phosphate buffer saline (PBS) solution kept at orbital shaking incubator.

2.9 Erythrocyte compatibility -Hemolysis test:

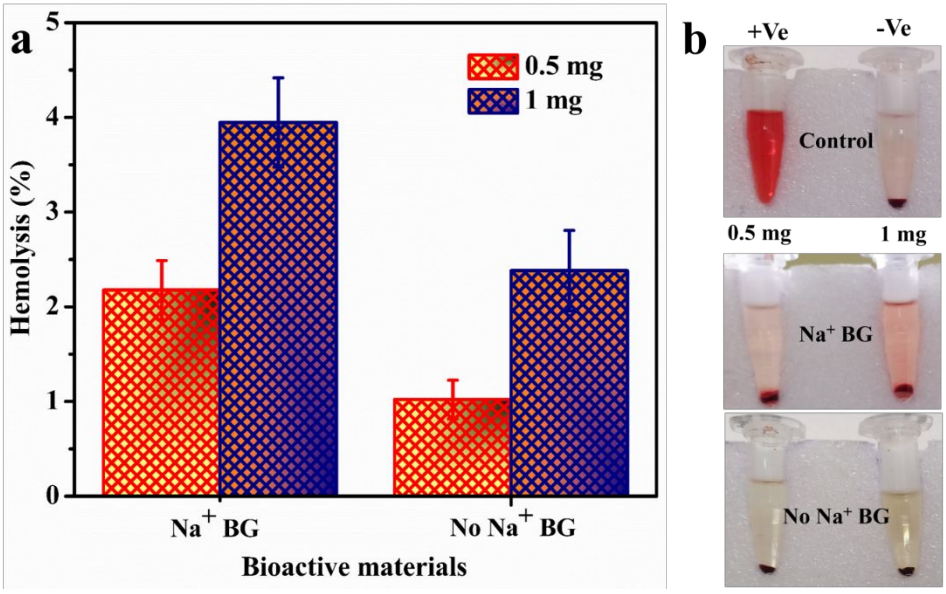

Figure S6. a) Hemocompatibility Assay of Na^+ BG and No Na^+ BG; b)Biomaterials showing less RBC lysis confirmed through clear solution after centrifugation.

2.10 Hemoclot Assay

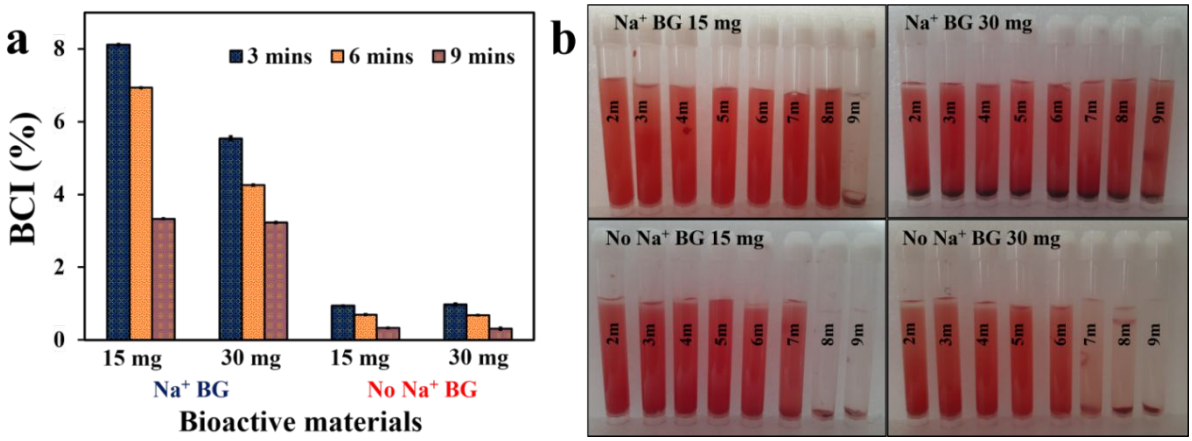

Figure S7. a) Hemoclot Assay showing BCI (%) of prepared BG; b) Resultant Color gradient over minutes projecting clot formation induced by prepared biomaterials.

Supplementary References:

1. Kokubo T, Ito S, Huang ZT, Hayashi T, Sakka S, Kitsugi T, Yamamuro T. Ca, P-rich layer formed on high-strength bioactive glass-ceramic A-W. *J. Biomed. Mater. Res.* **1990**,(3):331-43.
2. Chitra S, Bargavi P, Durgalakshmi D, Rajashree P, Balakumar S. Role of sintering temperature dependent crystallization of bioactive glasses on erythrocyte and cytocompatibility, *Process. Appl. Ceram. P.* **2019**, 13 (1):12-23.
3. Lefebvre L, Chevalier J, Gremillard L, Zenati R, Thollet G, Bernache-Assolant D, Govin A. Structural transformations of bioactive glass 45S5 with thermal treatments. *Acta Mater*. **2007**, 55(10):3305-13.
4. Lombardi M, Gremillard L, Chevalier J, Lefebvre L, Cacciotti I, Bianco A, Montanaro L. A comparative study between melt-derived and sol-gel synthesized 45S5 bioactive glasses. *Key Eng. Mater*. **2013**, 541, 15-30.
5. da Silva Buriti J, Barreto ME, Barbosa FC, de Brito Buriti BM, de Lima Souza JW, de Vasconcelos Pina H, de Luna Rodrigues P, Fook MV. Synthesis and characterization of Ag-doped 45S5 bioglass and chitosan/45S5-Ag biocomposites for biomedical applications. *J. Therm. Anal. Calorim. J.* **2021**, 145(1):39-50.
6. Chatzistavrou X, Zorba T, Kontonasaki E, Chrissafis K, Koidis P, Paraskevopoulos KM. Following bioactive glass behavior beyond melting temperature by thermal and optical methods, *Phys. Status Solidi A***. 2004**, 201(5):944-51.
7. Chen J, Wen Z, Zhong S, Wang Z, Wu J, Zhang Q. Synthesis of hydroxyapatite nanorods from abalone shells via hydrothermal solid-state conversion. *Mater. Des.* **2015**, 87:445-9.
8. Mukundan LM, Nirmal R, Vaikkath D, Nair PD. A new synthesis route to high surface area sol gel bioactive glass through alcohol washing: a preliminary study. *Biomatter.* **2013**, 3(2).
9. Bakhtiyari SS, Karbasi S, Monshi A. Evaluation of the effects of nano-TiO_2 on physical and mechanical properties of nano-bioglass 45S5 scaffold for bone tissue engineering. *Sci. Iran. SCI IRAN.* **2015,** 22(3):1337.
10. Stanciu GA, Sandulescu I, Savu B, Stanciu SG, Paraskevopoulos KM, Chatzistavrou X, Kontonasaki E, Koidis P. Investigation of the hydroxyapatite growth on bioactive glass surface. *j. biomed. pharm. sci.* **2007**;1(1):34-9.
11. Boccaccini AR, Chen Q, Lefebvre L, Gremillard L, Chevalier J. Sintering, crystallisation and biodegradation behaviour of Bioglass®-derived glass–ceramics. *Faraday Discuss.* **2007**,136, 27-44.
12. Karmakar B. Fundamentals of glass and glass nanocomposites. In Glass Nanocomposites. *William Andrew Publishing*, **2016**, 3-53.

13. Nandiyanto AB, Oktiani R, Ragadhita R. How to read and interpret FTIR spectroscope of organic material. *Indones. J. Sci. Technol.* **2019**, (1):97-118.
14. Er-Rouissi, Y., Aqdim, S., El Bouari, A., Hmimid, F. and Aqdim, S. Chemical Durability, Structure Properties and Bioactivity of Glasses $48P_2O_5$-30CaO-$(22- x)$ Na_2O-$xTiO_2$ (With $0< x\leq 3$; mol %). *Advances in Materials Physics and Chemistry*. **2020**, *10*(12), 305-318.
15. Filgueiras MR, La Torre G, Hench LL. Solution effects on the surface reactions of three bioactive glass compositions**.** *J. Biomed. Mater. Res.* **1993**, (12):1485-93.
16. El Batal HA, Azooz MA, Khalil EM, Monem AS, Hamdy YM. Characterization of some bioglass–ceramics. *Mater. Chem. Phys.* **2003**, 80(3):599-609.
17. Cacciotti I, Lombardi M, Bianco A, Ravaglioli A, Montanaro L. Sol–gel derived 45S5 bioglass: synthesis, microstructural evolution and thermal behaviour. *J. Mater. Sci.: Mater. Med.* **2012** (8), 1849-66.
18. Ray S, Dasgupta S. First principle study on in-vitro antimicrobial properties of nano 52S4. 6 bioactive glass. *Ceram.* **2020**, 46(9):13886-92.
19. Zheng K, Solodovnyk A, Li W, Goudouri OM, Stähli C, Nazhat SN, Boccaccini AR. Aging time and temperature effects on the structure and bioactivity of gel-derived 45S5 glass-ceramics. *J. Am. Ceram. Soc.* **2015**, 98(1):30-8.
20. Chen X, Chen X, Brauer DS, Wilson RM, Law RV, Hill RG, Karpukhina N. Sodium is not essential for high bioactivity of glasses. *Int. J. Appl. Glass Sci,* **2017**;8(4):428-37.
21. Bingel L, Groh D, Karpukhina N, Brauer DS. Influence of dissolution medium pH on ion release and apatite formation of Bioglass® 45S5. *Mater. Lett,* **2015**, 143:279-82.
22. Aguilar-Reyes, E.A., León-Patiño, C.A., Villicaña-Molina, E., Macías-Andrés, V.I. and Lefebvre, L.P., 2017. Processing and in vitro bioactivity of high-strength 45S5 glass-ceramic scaffolds for bone regeneration. *Ceram. 43*(9),6868-6875.
23. Azami M, Moztarzadeh F, Tahriri M. Preparation, characterization and mechanical properties of controlled porous gelatin/hydroxyapatite nanocomposite through layer solvent casting combined with freeze-drying and lamination techniques. *J. Porous Mater,* **2010,** (3):313-20.
24. Lin CC, Chen SF, Leung KS, Shen P. Effects of CaO/P2O5 ratio on the structure and elastic properties of SiO2–CaO–Na2O–P2O5 bioglasses. *J. Mater. Sci.: Mater. Med,* **2012**, (2):245-58.
25. Aguiar H, Serra J, González P, León B. Structural study of sol–gel silicate glasses by IR and Raman spectroscopies. *J. Non-Cryst. Solids*, **2009**, 355(8):475-80.
26. Matousek P, Morris M. Emerging Raman applications and techniques in biomedical and pharmaceutical fields. *Springer Science & Business Media*. **2010**, 347-364.

27. Amudha S, Ramya JR, Arul KT, Deepika A, Sathiamurthi P, Mohana B, Asokan K, Dong CL, Kalkura SN. Enhanced mechanical and biocompatible properties of strontium ions doped mesoporous bioactive glass. *Compos. B. Eng*, **2020**, 1; 196:108099.
28. Araújo M, Miola M, Baldi G, Perez J, Verné E. Bioactive glasses with low Ca/P ratio and enhanced bioactivity. *Mater,* **2016** (4):226.
29. Catauro M, Papale F, Sapio L, Naviglio S. Biological influence of Ca/P ratio on calcium phosphate coatings by sol-gel processing. *Mater. Sci. Eng. C,* **2016** 1; 65:188-93.
30. Zhou Z, Ruan J, Zou J, Zhou Z. Preparation and bioactivity of sol-gel macroporous bioactive glass. *Int. J. Miner. Metall. Mater,* **2008**, (3):290-6.
31. Hill RG, Brauer DS. Predicting the bioactivity of glasses using the network connectivity or split network models, *J. Non-Cryst. Solids,* **2011** 1;357(24):3884-7.
32. Wallace KE, Hill RG, Pembroke JT, Brown CJ, Hatton PV. Influence of sodium oxide content on bioactive glass properties. *J. Mater. Sci.: Mater. Med,* **1999** (12):697-701.
33. Babou-Kammoe R, Hamoudi S, Larachi F, Belkacemi K. Synthesis of CaCO3 nanoparticles by controlled precipitation of saturated carbonate and calcium nitrate aqueous solutions. **Can. J. Chem. Eng.**. 2012, 90(1):26-33.